EUROPEAN ORGANISATION FOR NUCLEAR RESEARCH

CERN-PPE/90-150
13 October 1990.

Search for the Minimal Standard Model Higgs Boson in e^+e^- Collisions at LEP

The OPAL Collaboration

Abstract

A search for the minimal Standard Model Higgs boson (H^0) has been performed with data from e^+e^- collisions in the OPAL detector at LEP. The analysis is based on approximately 8 pb^{-1} of data taken at centre-of-mass energies between 88.2 and 95.0 GeV. The search concentrated on the reaction $e^+e^- \rightarrow (e^+e^-,\ \mu^+\mu^-,\ \nu\bar{\nu}$ or $\tau^+\tau^-)H^0$, $H^0 \rightarrow (q\bar{q}$ or $\tau^+\tau^-)$ for Higgs boson masses above 25 GeV/c^2. No Higgs boson candidates have been observed. The present study, combined with previous OPAL publications, excludes the existence of a Standard Model Higgs boson with mass in the range $3 < m_{H^0} < 44$ GeV/c^2 at the 95% confidence level.

(Submitted to Phys. Lett.)

The OPAL Collaboration

M.Z. Akrawy[11], G. Alexander[21], J. Allison[14], P.P. Allport[5], K.J. Anderson[8], J.C. Armitage[6], G.T.J. Arnison[18], P. Ashton[14], G. Azuelos[16,J], J.T.M. Baines[14], A.H. Ball[15], J. Banks[14], G.J. Barker[11], R.J. Barlow[14], J.R. Batley[5], A. Beck[21], J. Becker[9], T. Behnke[7], K.W. Bell[18], G. Bella[21], S. Bethke[10], O. Biebel[3], U. Binder[9], I.J. Bloodworth[1], P. Bock[10], H. Breuker[7], R.M. Brown[18], R. Brun[7], A. Buijs[7], H.J. Burckhart[7], P. Capiluppi[2], R.K. Carnegie[6], A.A. Carter[11], J.R. Carter[5], C.Y. Chang[15], D.G. Charlton[7], J.T.M. Chrin[14], P.E.L. Clarke[23], I. Cohen[21], W.J. Collins[5], J.E. Conboy[13], M. Couch[1], M. Coupland[12], M. Cuffiani[2], S. Dado[20], G.M. Dallavalle[2], P. Debu[19], M.M. Deninno[2], A. Dieckmann[10], M. Dittmar[4], M.S. Dixit[17], E. Duchovni[24], I.P. Duerdoth[7,d], D.J.P. Dumas[6], P.A. Elcombe[5], P.G. Estabrooks[6], E. Etzion[21], F. Fabbri[2], P. Farthouat[19], H.M. Fischer[3], D.G. Fong[15], M.T. French[18], C. Fukunaga[22], A. Gaidot[19], O. Ganel[24], J.W. Gary[10], J. Gascon[16], N.I. Geddes[18], C.N.P. Gee[18], C. Geich-Gimbel[3], S.W. Gensler[8], F.X. Gentit[19], G. Giacomelli[2], V. Gibson[5], W.R. Gibson[11], J.D. Gillies[18], J. Goldberg[20], M.J. Goodrick[5], W. Gorn[4], D. Granite[20], E. Gross[24], J. Grunhaus[21], H. Hagedorn[9], J. Hagemann[7], M. Hansroul[7], C.K. Hargrove[17], I. Harrus[20], J. Hart[5], P.M. Hattersley[1], M. Hauschild[7], C.M. Hawkes[7], E. Heflin[4], R.J. Hemingway[6], R.D. Heuer[7], J.C. Hill[5], S.J. Hillier[1], C. Ho[4], J.D. Hobbs[8], P.R. Hobson[23], D. Hochman[24], B. Holl[7], R.J. Homer[1], S.R. Hou[15], C.P. Howarth[13], R.E. Hughes-Jones[14], R. Humbert[9], P. Igo-Kemenes[10], H. Ihssen[10], D.C. Imrie[23], L. Janissen[6], A. Jawahery[15], P.W. Jeffreys[18], H. Jeremie[16], M. Jimack[7], M. Jobes[1], R.W.L. Jones[11], P. Jovanovic[1], D. Karlen[6], K. Kawagoe[22], T. Kawamoto[22], R.G. Kellogg[15], B.W. Kennedy[13], C. Kleinwort[7], D.E. Klem[17], G. Knop[3], T. Kobayashi[22], T.P. Kokott[3], L. Köpke[7], R. Kowalewski[6], H. Kreutzmann[3], J. Kroll[8], M. Kuwano[22], P. Kyberd[11], G.D. Lafferty[14], F. Lamarche[16], W.J. Larson[4], J.G. Layter[4], P. Le Du[19], P. Leblanc[16], A.M. Lee[15], M.H. Lehto[13], D. Lellouch[7], P. Lennert[10], L. Lessard[16], L. Levinson[24], S.L. Lloyd[11], F.K. Loebinger[14], J.M. Lorah[15], B. Lorazo[16], M.J. Losty[17], J. Ludwig[9], J. Ma[4,b], A.A. Macbeth[14], M. Mannelli[7], S. Marcellini[2], G. Maringer[3], A.J. Martin[11], J.P. Martin[16], T. Mashimo[22], P. Mättig[7], U. Maur[3], T.J. McMahon[1], J.R. McNutt[23], F. Meijers[7], D. Menszner[10], F.S. Merritt[8], H. Mes[17], A. Michelini[7], R.P. Middleton[18], G. Mikenberg[24], J. Mildenberger[6], D.J. Miller[13], C. Milstene[21], M. Minowa[22], W. Mohr[9], A. Montanari[2], T. Mori[22], M.W. Moss[14], P.G. Murphy[14], W.J. Murray[5], B. Nellen[3], H.H. Nguyen[8], M. Nozaki[22], A.J.P. O'Dowd[14], S.W. O'Neale[7,c], B.P. O'Neill[4], F.G. Oakham[17], F. Odorici[2], M. Ogg[6], H. Oh[4], M.J. Oreglia[8], S. Orito[22], J.P. Pansart[19], G.N. Patrick[18], S.J. Pawley[14], P. Pfister[9], J.E. Pilcher[8], J.L. Pinfold[24], D.E. Plane[7], B. Poli[2], A. Pouladdej[6], E. Prebys[7], T.W. Pritchard[11], G. Quast[7], J. Raab[7], M.W. Redmond[8], D.L. Rees[1], M. Regimbald[16], K. Riles[4], C.M. Roach[5], S.A. Robins[11], A. Rollnik[3], J.M. Roney[8], S. Rossberg[9], A.M. Rossi[2,a], P. Routenburg[6], K. Runge[9], O. Runolfsson[7], S. Sanghera[6], R.A. Sansum[18], M. Sasaki[22], B.J. Saunders[18], A.D. Schaile[9], O. Schaile[9], W. Schappert[6], P. Scharff-Hansen[7], S. Schreiber[3], J. Schwarz[9], A. Shapira[24], B.C. Shen[4], P. Sherwood[13], A. Simon[3], P. Singh[11], G.P. Siroli[2], A. Skuja[15], A.M. Smith[7], T.J. Smith[1], G.A. Snow[15], R.W. Springer[15], M. Sproston[18], K. Stephens[14], H.E. Stier[9], R. Strohmer[10], D. Strom[8], H. Takeda[22], T. Takeshita[22], P. Taras[16], N.J. Thackray[1], T. Tsukamoto[22], M.F. Turner[5], G. Tysarczyk-Niemeyer[10], D. Van den plas[16], G.J. VanDalen[4], G. Vasseur[19], C.J. Virtue[17], H. von der Schmitt[10], J. von Krogh[10], A. Wagner[10], C. Wahl[9], J.P. Walker[1], C.P. Ward[5], D.R. Ward[5], P.M. Watkins[1], A.T. Watson[1], N.K. Watson[1], M. Weber[10], S. Weisz[7], P.S. Wells[7], N. Wermes[10], M. Weymann[7], G.W. Wilson[19], J.A. Wilson[1], I. Wingerter[7], V-H. Winterer[9], N.C. Wood[13], S. Wotton[7], B. Wuensch[3], T.R. Wyatt[14], R. Yaari[24], Y. Yang[4,b], G. Yekutieli[24], T. Yoshida[22], W. Zeuner[7], G.T. Zorn[15].

[1]School of Physics and Space Research, University of Birmingham, Birmingham, B15 2TT, UK
[2]Dipartimento di Fisica dell' Università di Bologna and INFN, Bologna, 40126, Italy

[3]Physikalisches Institut, Universität Bonn, D-5300 Bonn 1, FRG
[4]Department of Physics, University of California, Riverside, CA 92521 USA
[5]Cavendish Laboratory, Cambridge, CB3 0HE, UK
[6]Carleton University, Dept of Physics, Colonel By Drive, Ottawa, Ontario K1S 5B6, Canada
[7]CERN, European Organisation for Particle Physics, 1211 Geneva 23, Switzerland
[8]Enrico Fermi Institute and Department of Physics, University of Chicago, Chicago Illinois 60637, USA
[9]Fakultät für Physik, Albert Ludwigs Universität, D-7800 Freiburg, FRG
[10]Physikalisches Institut, Universität Heidelberg, Heidelberg, FRG
[11]Queen Mary and Westfield College, University of London, London, E1 4NS, UK
[12]Birkbeck College, London, WC1E 7HV, UK
[13]University College London, London, WC1E 6BT, UK
[14]Department of Physics, Schuster Laboratory, The University, Manchester, M13 9PL, UK
[15]Department of Physics and Astronomy, University of Maryland, College Park, Maryland 20742, USA
[16]Laboratoire de Physique Nucléaire, Université de Montréal, Montréal, Quebec, H3C 3J7, Canada
[17]National Research Council of Canada, Herzberg Institute of Astrophysics, Ottawa, Ontario K1A 0R6, Canada
[18]Rutherford Appleton Laboratory, Chilton, Didcot, Oxfordshire, OX11 0QX, UK
[19]DPhPE, CEN Saclay, F-91191 Gif-sur-Yvette, France
[20]Department of Physics, Technion-Israel Institute of Technology, Haifa 32000, Israel
[21]Department of Physics and Astronomy, Tel Aviv University, Tel Aviv 69978, Israel
[22]International Centre for Elementary Particle Physics and Dept of Physics, University of Tokyo, Tokyo 113, and Kobe University, Kobe 657, Japan
[23]Brunel University, Uxbridge, Middlesex, UB8 3PH UK
[24]Nuclear Physics Department, Weizmann Institute of Science, Rehovot, 76100, Israel

[a]Present address: Dipartimento di Fisica, Università della Calabria and INFN, 87036 Rende, Italy
[b]On leave from Harbin Institute of Technology, Harbin, China
[c]Now at Applied Silicon Inc
[d]On leave from Manchester University
[e]On leave from Birmingham University
[f]and TRIUMF, Vancouver, Canada

1 Introduction

Spontaneous symmetry breaking is a cornerstone of the Standard Model of electroweak interactions [1]. In local gauge invariant theories of electroweak interactions, spontaneous symmetry breaking requires the existence of one or more scalar particles, the Higgs boson(s) [2]. However, while the Standard Model has been successful in describing many processes to a high degree of accuracy, these particles have not been observed. In the minimal Standard Model, one complex doublet of Higgs fields is introduced, which results in a single scalar Higgs boson (H^0) with an unspecified mass, that has well defined couplings to pointlike bosons and fermions. A Higgs boson with a mass (m_{H^0}) in the ranges of $0 < m_{H^0} < 0.2$ GeV/c^2 and $3.0 < m_{H^0} < 25.3$ GeV/c^2 has already been excluded in earlier publications [3,4] by this collaboration. To date, the limits presented by this and other experiments exclude the mass range $0 < m_{H^0} < 41.6$ GeV/c^2 at the 95% confidence level [3,4,5,6,7,8,9].

In the present analysis a search for Higgs bosons was performed using data accumulated during the 1989 and the 1990 scan of the Z^0 resonance; this corresponds to an integrated luminosity of 8.0 pb^{-1}, or about 170,000 reconstructed multihadron events. The energies and integrated luminosities are listed in table 1. In the minimal Standard Model a Higgs boson can be produced in e^+e^- collisions near the Z^0 resonance in association with a virtual Z^{0*}. For the searches presented here, the Higgs boson would decay predominantly into $b\bar{b}, c\bar{c}$, or $\tau^+\tau^-$, which are the most massive particles kinematically accessible in the mass range considered. The decays involving $Z^{0*} \rightarrow (\nu\bar{\nu},\ e^+e^-$ or $\mu^+\mu^-)$ have been selected for this study since final states with large missing momentum or isolated lepton pairs are very distinctive. The final state $\tau^+\tau^-$-*jet-jet* has been studied for Higgs boson masses above 25 GeV/c^2 as it too gives a distinctive signal, albeit with a lower search efficiency.

Previous searches for Higgs bosons in the channel $\nu\bar{\nu}H^0$ performed by this collaboration [4,5], optimised for lower masses, concentrated on a monojet-like topology. This kind of search has a lower efficiency for larger m_{H^0} since a more massive Higgs boson would decay primarily into two b-jets with a large opening angle between them. In the present search, a higher efficiency was achieved for $m_{H^0} > 25$ GeV/c^2 by using the acollinear characteristics expected for the jets produced in the decay of a boosted H^0, as well as the fact that the jets from b-quark fragmentation have a mass in a well defined range. This search made use of the high hermeticity and good total energy resolution of the OPAL detector which is possible when the information from its central tracking chamber, electromagnetic and hadron calorimeters is combined. Since this analysis uses the hadron calorimeter, it has not been applied to the first 6.6% of the data, for which the hadron calorimeter information was not available. Instead, for this first 6.6% of the data ($OLD_{\nu\bar{\nu}H^0}$ in table 1), the analysis described in the previous publication [4] was used.

The new analysis of the reaction $e^+e^- \rightarrow (e^+e^-$ or $\mu^+\mu^-)H^0$ improves on the previous publication by combining the isolation requirements on the leptons with the lepton identification capabilities of the OPAL detector. Since these capabilities were improved after the 1989 data taking period, the new analysis could not be applied to the 1989 data; instead, the analysis previously published [4] is used for that data ($OLD_{l^+l^-H^0}$ in table 1). The $\tau^+\tau^-$-*jet-jet* analysis is based on the method described in the previous publication [4], however changes were introduced to increase its efficiency for m_{H^0} above 40 GeV/c^2.

2 The OPAL Detector

The data were recorded at the CERN e^+e^- collider LEP during 1989 and 1990 using the OPAL detector [10], which is a multipurpose apparatus having nearly 4π steradians acceptance. The central detector consists of a system of tracking chambers inside a 0.435 Tesla solenoidal magnetic volume. The central detector system is surrounded by a time of flight counter array, a lead glass electromagnetic calorimeter (EM) with a presampler, an instrumented magnet return yoke serving as a hadron calorimeter, four layers of outer muon chambers, and an endcap system which includes a low-angle forward detector.

The central tracking detector consists of a precision vertex chamber, a large volume "jet" chamber, and chambers for tracking in the $r-\theta$ plane (the coordinate system is defined with z along the beam axis, θ and ϕ being the polar and azimuthal angles). The main tracking is done with the jet chamber, a drift chamber of approximately four metre length and two metre radius, with 24 sectors in ϕ and 159 layers of sense-wires in each sector. Tracks having $|\cos\theta| \leq 0.97$ ($|\cos\theta| \leq 0.93$) give a minimum of 20 (40) possible hits in the jet chamber.

The electromagnetic calorimeter consists of a cylindrical array of 9440 lead glass blocks of 24.6 radiation lengths thickness covering the range $|\cos\theta| < 0.82$, and 2264 lead glass blocks of 20 radiation lengths thickness in the endcaps covering the region between $0.81 < |\cos\theta| < 0.98$. Each block subtends a solid angle of approximately 40×40 mrad^2 and projects towards a point near the interaction point in the barrel region and along the beam direction in the endcaps. The three sections of the electromagnetic calorimeter cover 98% of the solid angle.

The hadron calorimeter is divided into a barrel region ($|\cos\theta| < 0.81$), a pair of annular endcaps ($0.81 < |\cos\theta| < 0.91$) and a pair of pole tip sections ($0.91 < |\cos\theta| < 0.99$). The barrel (endcap) consists of 9 (8) layers of limited streamer tubes, alternating with 8 (7) iron slabs for a total of 4.8 (4.2) interaction lengths. Layers are grouped to form towers that project towards the interaction point with each tower subtending approximately 7.5° in ϕ and 5° in θ. Signals induced on 4 mm wide strips which run the full length of each limited streamer tube are also read out to provide precise $r-\phi$ (vertical) tracking information through the barrel (endcap) calorimeter. In the pole tip there are 10 layers of thin high gain multiwire chambers alternating with 9 iron slabs for a total of 4.3 interaction lengths. Towers here extend 11° in ϕ and 4° in θ and the strips provide radial tracking information.

The muon system surrounds the OPAL magnet yoke and is constructed as a barrel and two endcaps. The barrel detector consists of four layers of planar drift chambers covering the region $|\cos\theta| \lesssim 0.68$ while the endcap detectors are composed of four layers of limited streamer tube chambers and cover the range $0.67 \lesssim |\cos\theta| \lesssim 0.98$. There are at least 7 interactions lengths of material between the interaction point and the muon detectors for most of the solid angle covered by the muon system. Of the full solid angle, 88% is covered by at least three layers of detectors.

The luminosity of the colliding beams was determined by observing small angle Bhabha scattering with the forward detector, a lead-scintillator calorimeter with associated tracking chambers at either end of the central detector with an acceptance covering $40 < \theta < 150$ mrad in the polar angle and 2π in azimuth. This device currently provides a luminosity measurement with a systematic accuracy of better than 2.2% [11].

3 Global Event Selection and Quality Cuts

The following quality requirements have been imposed on tracks used in the event analysis:

- $|d_0| < 2.5$ cm, where $|d_0|$ is the distance of closest approach to the beam axis in a plane perpendicular to the beam axis.
- $|z_0| < 50$ cm, where $|z_0|$ is the distance of closest approach to the interaction point, along the beam axis.
- $N_{hit} > 20$, corresponding to $|\cos\theta| < 0.97$, where N_{hit} is the number of hits in the jet chamber along the charged track. It was further required that the track contain more than 50% of the hits expected for its polar angle. For the 1989 data, $N_{hit} > 40$, corresponding to $|\cos\theta| < 0.93$, was demanded.
- $p_t > 100$ MeV/c, where p_t is the track momentum component perpendicular to the beam direction.

Electromagnetic clusters consisted of groups of contiguous lead glass blocks, where each block registered more than 20 MeV. A cluster was required to have a minimum energy of 170 MeV in the barrel and 250 MeV in the endcap region. Endcap clusters were required to contain a minimum of two adjacent blocks. Hadron calorimeter clusters were made of single towers containing an energy in excess of 600 MeV in the barrel and endcap regions, and 3 GeV in the pole tips.

For the event selection, it was demanded that the tracking chambers, forward detectors, electromagnetic and hadron calorimeters be fully operational.

Since the present analysis is intended for Higgs bosons with mass above 25 GeV/c^2, which decay mainly into high multiplicity final states, it was further demanded that:

- $N_{good} > 5$, where N_{good} is the number of charged tracks passing the quality requirements described above.
- $N_{EM} > 5$, where N_{EM} is the number of EM clusters satisfying the above requirements.
- There was at least one track with $p_t > 1$ GeV/c.

In order to reduce the background from beam gas and beam wall interactions, which contain a large number of tracks not coming from the interaction point, the following requirement was imposed:

- $N_{good}/N_{all} > 0.20$, where N_{all} is the total number of reconstructed charged tracks in the event.

Finally, in order to reduce the background from two-photon events, it was demanded that:

- $E_{FD} < 2$ GeV, where E_{FD} is the energy deposited in the forward detectors.

4 Missing Energy Search

The missing energy search was directed towards events of the type $e^+e^- \to Z^{0*}H^0$, $Z^{0*} \to \nu\bar{\nu}$, $H^0 \to q\bar{q}$ which are characterized by a significant momentum imbalance in the event. To estimate the missing energy and momentum of an event, an algorithm was developed to compute the total 4-momentum

of the event from the measured tracks and clusters. First, the 4-momenta of all charged tracks and clusters were summed. A subtraction was then made for each charged track in order to correct for double counting. The subtraction amounted to the average energy (as computed in a Monte Carlo simulation of the detector) deposited in the lead glass and hadron calorimeter by a charged pion having the same momentum as that of the track. After applying the general quality requirements, the following preselection cuts (A0 in table 2) were imposed to ensure event containment and to remove obvious backgrounds:

- Less than 35% of the EM energy was contained in both cones around the beam direction satisfying $|\cos\theta_{EM}| > 0.90$. This cut removed forward going events as well as 3-jet events where one or more jets were produced along the beam direction. This selection used only the EM calorimeter to take advantage of its more uniform response in this region, as compared to other detector elements.

- $|\cos\theta_{p_{miss}}| < 0.90$, where p_{miss} is the missing momentum vector described above. This requirement reduced the contamination from two-photon and radiative events.

- $Thrust < 0.95$ for events containing fewer than nine charged tracks. The thrust was calculated using charged tracks, electromagnetic and hadronic calorimeter clusters. This requirement eliminated virtually all the tau pair events.

Fig. 1a shows the measured mass of the remaining events normalized to the centre-of-mass energy. It can be seen that the bulk of the events was due to multihadron decays of the Z^0 boson accompanied by some two-photon contribution at low values of the normalized mass. The data above 0.2 are well reproduced, both in absolute magnitude and shape, by the Monte Carlo that describes the multihadron decays of the Z^0. This Monte Carlo is based on the GEANT [12,13] package and uses the Jetset 7.2 Monte Carlo [14] as its generator. The 1.5% shift between the Monte Carlo and the data distributions is primarily due to the imperfect simulation of tracks which point in the forward direction.

Events were divided into two hemispheres along the thrust axis, and the momentum direction in each hemisphere was calculated using charged tracks and clusters with the algorithm described above. For each of the following requirements (A1 to A5) the calculations of energies and momenta were performed in two ways, first using hadronic clusters as well as electromagnetic clusters and charged tracks, and then using electromagnetic clusters and charged tracks only. In each case the subtraction for the double counting of charged tracks was performed accordingly. This procedure was followed because the resolution in energies and angles is less precise for the hadron calorimeter than for the other devices. Although the hadron calorimeter is essential for obtaining a good measurement of events with energetic neutral hadrons, its inclusion slightly degraded the resolutions for other classes of events, such as two-photon events. As a consequence, each of the following cuts was applied to the quantities calculated both with and without the hadron calorimeter, and the event was rejected if it failed either cut (had one applied all the cuts using the hadron calorimeter in all calculations, the final results would be unchanged).

In order to suppress the multihadron background and exploit the acollinear topology of the $\nu\bar{\nu}ll^0$ final state, the following two cuts were applied to all events in which the energy of each hemisphere was measured to be at least 3 GeV:

- (A1) $\theta_{acop} > 16°$, where $180° - \theta_{acop}$ is the angle between the momentum vectors of the hemispheres projected on a plane perpendicular to the beam direction.

- (A2) $\theta_{acol} > 26°$, where $180° - \theta_{acol}$ is the angle between the momentum vectors of the hemispheres.

Events with less than 3 GeV in one hemisphere were retained, at this stage of the analysis, as monojet candidates.

The distributions of θ_{acop} (before cut A1) and θ_{acol} (after cut A1), are shown in fig. 2 for the data, the multihadron Monte Carlo, and the expected Higgs boson signal with $m_{H^0} = 40$ GeV/c^2. The values of θ_{acop} and θ_{acol} are the lesser of the values obtained with and without the hadron calorimeter.

Fig. 1b shows the normalized mass distribution for the events which remain. This distribution can be characterized by two populations, one of low mass two-photon events and the other of high mass multi-jet events. To further reduce the two-photon and multihadronic Z^0 background, additional cuts were imposed:

- (A3) $p_T > 6$ GeV/c, where p_T is the transverse momentum of the event with respect to the beam direction. This cut eliminated all the remaining two-photon events.

- (A4) $E_{30} < 2$ GeV, where E_{30} is the scalar sum of track momenta and cluster energies within a cone of 30° half angle, oriented along the missing momentum direction. This requirement has almost no effect on the $\nu\bar{\nu}H^0$ events, but eliminates most of the quasi-collinear events, resulting from mismeasured multi-jet events, or from events where a large amount of missing energy was carried by neutrinos originating from heavy flavour decays.

Fig. 1c shows the normalized mass distribution of the remaining events. There are no events with a normalized mass below 0.62. The selected events are incompatible with a Higgs boson signal for $m_{H^0} \lesssim 50$ GeV/c^2. This can be seen in fig. 1d, which shows the narrow normalized mass distribution expected for a Higgs boson with $m_{H^0} = 40$ GeV/c^2 after the above requirements. However, in order to retain sensitivity to Higgs bosons with higher mass, no cut on the normalized mass has been applied.

The remaining events are mainly three and four jet events, with large masses in at least one hemisphere. This is consistent with the Jetset 7.2 Monte Carlo prediction. However, this would not be the case for a high mass Higgs boson, which decays into heavy quarks with a hard fragmentation, leading to lower mass jets. Thus, the following cuts were applied:

- (A5) $(M_{hemi1} + M_{hemi2})/2 < 12.5$ GeV/c^2 or $E_{hemi2} < 3$ GeV, where the hemispheres are labelled by $E_{hemi1} > E_{hemi2}$. The second requirement selects monojets, while the first demands that the average mass of the two jets be consistent with that of hard fragmenting b-jets. Fig. 3 shows the average of M_{hemi1} and M_{hemi2} for the data and for a hypothetical Higgs boson of $m_{H^0} = 40$ GeV/c^2, after applying cuts A(1) to A(4). It can be seen that the remaining events in the data (mainly four jet events) have high average masses, while almost all the expected Higgs boson events have an average hemisphere mass below 12.5 GeV/c^2.

After applying the above requirements (see table 2 for the number of events surviving each cut) no events were left in the data. The efficiency reduction due to each of the above requirements is given in table 2. It can be seen that the last requirement has negligible influence on the efficiency but removes the high mass background events. Furthermore, high statistics Monte Carlo studies have shown that the background does not appear to accumulate at high visible masses. Consequently, this analysis has the potential to be extended to higher masses when more data become available.

5 Search for $Z^0 \rightarrow (e^+e^-$ or $\mu^+\mu^-)H^0$

This analysis is based on a search for events with pairs of isolated electrons or muons. Events were selected from the sample defined in section 3, which is predominantly populated by hadronic decays of the Z^0. A small fraction of the events was from radiative leptonic decays of the Z^0 or tau pairs. These backgrounds were eliminated by requiring that there be at least four tracks outside of 15° cones around each of the two leptons.

A search was made for pairs of oppositely charged particles identified as an e^+e^- or $\mu^+\mu^-$ pair according to the lepton identification criteria listed below. The pair was required to have an opening angle greater than 30°, and each of the two tracks was required to have a momentum exceeding 5 GeV/c, a polar angle satisfying $|cos\theta| < 0.90$, and to be associated to an electromagnetic cluster. To maintain a high efficiency for muons, tracks associated with electromagnetic clusters with energies below the values given in section 3 were also accepted.

Using decays of the $Z^0 \rightarrow e^+e^-$ and $\mu^+\mu^-$, lepton identification criteria were chosen to identify lepton pairs with high efficiency. The quantities on which these criteria were based are well simulated by the Monte Carlo.

A good e^+e^- pair was required to satisfy each of the following conditions:

- Each of the two tracks had an associated electromagnetic energy of at least 5 GeV, with 90% of this energy contained in fewer than five lead glass blocks.
- The azimuthal angle of the extrapolated track and the associated electromagnetic cluster agreed to within 20 mrad.
- Any hadron calorimeter cluster associated with either track had an energy of less than 4 GeV.
- The sum of the two associated electromagnetic clusters was at least 25 GeV.

A good $\mu^+\mu^-$ pair was required to satisfy each of the following conditions:

- Each of the two tracks was associated with either: i) two or more hits in the muon chambers or ii) two or more strip hits in the outer five hadron calorimeter layers.
- At least one of the muon tracks was associated with either i) a track segment in the hadron calorimeter containing at least five layers of strips or ii) a track segment in the muon chambers containing at least 3 planes.
- The sum of the EM energy associated to the two tracks was less than 5 GeV.
- The scalar momentum sum of the two tracks was at least 25 GeV/c.

Each of the two candidate lepton tracks was required to be isolated from other particles in the event. If more than one candidate dilepton pair was found in an event, the pairs were ranked according to the total amount of charged energy (excluding the lepton track) and unassociated neutral energy in two cones of half angle 30° centred on the lepton tracks. The pair with the smallest sum in these two cones was considered for further analysis. A total of 245 events satisfied the above requirements (see table 3).

The event was required to have either two leptons, each isolated in a cone of half angle 30° centred on the track, or else a single high momentum lepton isolated within a cone of 45°. The

latter requirement is well suited for asymmetric decays of the Z^{0*} with a soft lepton near the Higgs boson decay products and an isolated hard lepton. An event passed cut B1 if either of the following conditions were true:

- (B1a) The total EM energy summed over both cones of half angle 30° about the two leptons was required to be less than 5 GeV. An identical cut was applied separately to the charged and hadron calorimeter energies. Each sum included the unassociated energy around both of the leptons as well as the associated EM energy in the case of muons, and the associated hadron calorimeter energy in the case of electrons.
- (B1b) Each of the sums of EM, charged and hadron calorimeter energy in a cone of half angle 45° about one lepton and a cone of 15° about the other lepton was required to be less than 5 GeV. The lepton in the 45° cone was required to have an energy exceeding 20 GeV. The unassociated EM and charged energies in the 15° cone were each required to be less than 1 GeV.

Fig. 4 shows the sums of EM and charged energies in the two 30° cones and in the combination of 15° and 45° cones for both data and the expectation for a Higgs boson with $m_{H^0} = 40$ GeV/c^2. The excluded regions are shown in the figure. While cut B1 eliminated all the events, background studies indicated that an additional isolation cut was required:

- (B2) The scalar sum of charged momenta in both cones of half angle 15° about the two leptons be less than 1 GeV/c. This requirement allows for final state radiation about the leptons, but discriminates against nearby stiff tracks.

A rough background estimate was performed by applying the above requirements without demanding lepton identification. Since the tracks in this background sample were not identified as muons or electrons, the EM and hadron calorimeter energies associated to the tracks could not be included in the energy sums of cut B1. A total of 21 events were selected from 24,581 events reducing the background by a factor of about 1200. Assuming that this rejection factor also applied to the sample of identified lepton pairs, the background from hadronic decays of the Z^0 was 0.21±0.04 (statistical error only). Table 3 gives the efficiency after each of the above requirements and table 4 gives the overall efficiency for various Higgs boson masses. These efficiencies have been calculated using a Monte Carlo generator based on ref. [15], which has been modified to include final state radiation from the leptons in the Z^{0*} decay, but not interference between initial and final state radiation, which is expected to be negligible. The efficiency as calculated from the Monte Carlo is multiplied by 0.98 to correct for inefficiencies in the charged track association to EM clusters, not included in the Monte Carlo.

6 Search for $Z^0 \to \tau^+\tau^-$ *jet jet*

In order to include most of the possible decay modes of the $Z^{0*}H^0$ system, a search for the final state $\tau^+\tau^-$*-jet-jet* was also performed. The analysis was based on the full integrated luminosity, since no use was made of the hadron calorimeter. The basic requirement was for high sphericity ($S > 0.1$), high charged multiplicity ($N_{good} > 7$) events, that contain a pair of isolated oppositely charged tracks. This pair of charged tracks was expected to come from the decay of the $\tau^+\tau^-$ system, where each tau decays into a final state containing a single charged track. Since the charged track from a tau-decay is often accompanied by unassociated neutral energy, which causes it to resemble a regular parton jet, further discrimination between multi-jet and $\tau^+\tau^-$*-jet-jet* events was required. This discrimination is partially based on the string effect [16], which characterizes QCD jets, and leads to the presence of soft particles between jets. Therefore, more stringent isolation requirements had to be imposed than in the dilepton search described in section 5. The requirements were:

- The track momentum should exceed 3 GeV/c for each of the tracks.
- There should be no additional good tracks within a cone of 30° half angle around each track.
- In an annular region between two cones of half angles 15° and 30° around each of the two tracks, there should be less than 0.5 GeV of EM energy.
- Each of the tracks should have a polar angle in the range $15° < \theta < 135°$. This requirement ensured that neither cone overlaped with the region excluded by the quality cuts around the beam direction, where soft particles could be missed. Such an isolation requirement was crucial to this search because soft particles between jets characterize QCD jets, while this is not the case for jet-like tau-decays.

After applying the above requirements, 186 events remained. For each of these events, the effective mass of the pair was less than 7.5 GeV/c^2. Since track pairs from either a Z^{0*} or a high mass Higgs boson, in this channel, would have typically large masses, a cut is applied at 10.0 GeV/c^2 leaving no events in the sample. Table 4 shows the efficiencies obtained when the $\tau^+\tau^-$-*jet-jet* search is applied to $H^0 \rightarrow \tau^+\tau^-$, $Z^{0*} \rightarrow$ *jet-jet* and $H^0 \rightarrow$ *jet-jet*, $Z^{0*} \rightarrow \tau^+\tau^-$, as well as the contribution to the expected number of events for different Higgs boson masses.

7 Systematic Uncertainties and Mass Limit

Two sources of systematic errors were common to all the analyses. These were:

- Luminosity: a conservative 2.2% systematic error has been estimated for the error on the luminosity measurement.
- Higgs boson cross section: a 2% systematic error has been used. The cross section calculation includes the improved Born approximation [17] and the top quark triangle graph at the $Z^0Z^{0*}H^0$ vertex [18], which due to cancellations, leads to a negligible dependence on the value of the top quark mass. A full description of this calculation can be found in ref. [4]. The decay branching ratios assumed for the Higgs boson include QCD corrections that were calculated following ref. [19]

For each of the individual reactions, the systematic errors have been evaluated separately. In the case of the missing energy channel, they are due to:

- B decay modelling: a 1.6% systematic error for Higgs boson masses near 45 GeV/c^2 has been estimated. This is based on the effect of the charged multiplicity cut, which if it were changed by one unit in the Monte Carlo, would lead to such an error.
- Fragmentation dependence: a 2% systematic error has been estimated for this dependence. This was obtained by studying the dependence of the hadronization process in Jetset 6.3 on the parameters Λ_{QCD}, Q_0, σ_q and a (a is one of the fragmentation parameters in the Lund "symmetric scheme") and alternatively ϵ_b (the Peterson fragmentation parameter), by the change in the acceptance for the channel $Z^0 \rightarrow H^0\nu\bar{\nu}$ as the Jetset parameters were each varied. The parameters Q_0, σ_q, and a were varied independently by one standard deviation, while all other parameters were held at their nominal values; the errors were taken from ref. [20]. The parameter Λ_{QCD} was increased by three standard deviations in order to study the effect of increased gluon radiation which might be the case for a scalar particle decay, in contrast to the expectation for a vector boson [19]. The Peterson fragmentation variable ϵ_b was varied between 0.02 and

0.005; this range of ϵ_b is relevant for the range of m_{H^0} under consideration in this analysis (see e.g. ref. [21]). The maximum deviation observed with respect to the value obtained using the nominal parameter values was 2%.

- Simulation of detector response: a 3% error was estimated by comparing two simulations that differ in their model of the calorimeter response.

In the case of the dilepton search ($\mu^+\mu^-$ or e^+e^-), the systematic errors due to the decay of the Higgs boson are of lesser importance since a charged multiplicity of at least four tracks is demanded for its decay and no demands are made that are sensitive to the fragmentation properties of its decay products. The main systematic error contributions come from the lepton identification demands. These can be itemized as:

- Simulation of detector response for isolated lepton pairs: a 1% error has been estimated from the comparison of the data and Monte Carlo simulations of Z^0 decays to electron and muon pairs.

- Effect of final state radiation of leptons: a conservative 1% error has been estimated by allowing for a 25% error in the simulation of final state radiation.

Adding the appropriate uncertainties in quadrature, one obtains a systematic error of 5% for each of the above searches. The systematic uncertainty for the decay $Z^0 \rightarrow \tau^+\tau^-$-*jet-jet* has been estimated in a previous publication ([4]) to be less than 10%. However, the relative contribution from this channel is very small.

The combined efficiencies for the published [4] and present analyses for each of the decay channels are given in table 4 for various Higgs boson masses. Also shown in the table are the expected numbers of events. The expected number of observed events reduced by one standard deviation in their respective systematic errors as a function of the Higgs boson mass are shown in fig. 5 for the combined analyses and for each of the decay channels. It can be seen from their sum, also shown, that a minimal Standard Model Higgs boson is excluded for $m_{H^0} < 44$ GeV/c^2 at the 95% confidence level.

8 Conclusions

Using 1989 and 1990 data, the existence of a minimal Standard Model Higgs boson has been excluded in the mass range of $3 < m_{H^0} < 44$ GeV/c^2 at the 95% confidence level, by using a combined analysis of the decays $H^0 \rightarrow (\tau^+\tau^-$ or $q\bar{q})$, $Z^{0*} \rightarrow (\nu\bar{\nu}$ or $\mu^+\mu^-$ or $e^+e^-)$ and $H^0Z^{0*} \rightarrow \tau^+\tau^-$ *jet-jet*. These searches were limited by the available statistics and the range of Higgs boson masses for which these analyses are sensitive should increase as this experiment accumulates more data.

9 Acknowledgments

It is a pleasure to thank the SL Division for the efficient operation of the LEP accelerator, the precise information on the absolute energy, and their continuing close cooperation with our experimental group. In addition to the support staff at our own institutions we are pleased to acknowledge the following :
Department of Energy, USA
National Science Foundation, USA

Science and Engineering Research Council, UK
Natural Sciences and Engineering Research Council,Canada
Israeli Ministry of Science
Minerva Gesellschaft
The Japanese Ministry of Education, Science and Culture (the Monbusho) and a grant under the Monbusho International Science Research Program
American Israeli Bi-national Science Foundation
Direction des Sciences de la Matière du Commissariat à l'Energie Atomique, France
The Bundesministerium für Forschung und Technologie, FRG
and The A.P. Sloan Foundation.

References

[1] S. L. Glashow, J. Iliopoulos and L. Maiani, Phys. Rev. **D2** (1970) 1285 ; S. Weinberg, Phys. Rev. Lett. **19** (1967) 1264; A. Salam, *Elementary Particle Theory*, ed. N. Svartholm (Almquist and Wiksells, Stockholm, 1969), p. 367.

[2] P. W. Higgs, Phys. Lett. **12** (1964) 132; F. Englert and R. Brout, Phys. Rev. Lett. **13** (1964) 321; G. S. Guralnik, C. R. Hagen, and T. W. B. Kibble, Phys. Rev. Lett. **13** (1964) 585.

[3] OPAL Collab., M. Z. Akrawy *et al.*, CERN-PPE/90-116 (1990) (submitted to Phys. Lett. B).

[4] OPAL Collab., M. Z. Akrawy *et al.*, CERN-EP/90-100 (1990) (submitted to Zeit. Phys. C).

[5] OPAL Collab., M. Z. Akrawy *et al.*, Phys. Lett. **B236** (1990) 224.

[6] ALEPH Collab., D. Decamp *et al.*, Phys. Lett. **B236** (1990) 233; ALEPH Collab., D. Decamp *et al.*, Phys. Lett. **B241** (1990) 141; ALEPH Collab., D. Decamp *et al.*, Phys. Lett. **B246** (1990) 306.

[7] DELPHI Collab., P. Abreu *et al.*, CERN-EP/90-44 (1990).

[8] ALEPH Collab., D. Decamp *et al.*, Phys. Lett. **B245** (1990) 289.

[9] L3 Collab., B. Adeva *et al.*, L3 preprint 10 (1990); L3 Collab., L3 preprint 19 (1990).

[10] OPAL Collab., K. Ahmet *et al.*, CERN-PPE/90-114 (1990) (submitted to Nucl. Instr. and Meth.)

[11] OPAL Collab., M. Z. Akrawy *et al.*, Phys. Lett. **B240** (1990) 497.

[12] R. Brun, F. Bruyant, M. Maire, A. C. McPherson and P. Zanarini, GEANT3, CERN DD/EE/84-1 (1987).

[13] J. Allison *et al.*, Comp. Phys. Comm. **47** (1987) 55.

[14] T. Sjostrand, Comp. Phys. Comm. **39** (1986) 347; T. Sjostrand, Comp. Phys. Comm. **43** (1987) 367; M. Bengtsson and T. Sjostrand, Nucl. Phys. **B289** (1987) 810.

[15] F.A. Berends and R. Kleiss, Nucl. Phys. **B260** (1985) 32.

[16] JADE Collab., W. Bartel *et al.*, Zeit. Phys. **C21** (1983) 37; TPC Collab., H. Aihara *et al.*, Zeit. Phys. **C28** (1985) 31.

[17] M. Consoli and W. Hollik, *Electroweak Corrections for Z^0 Physics*, in CERN 89-8, Vol. 1, p. 39.

[18] Z. Hioki, Phys. Lett. **B224** (1989) 417.

[19] E. Braaten and J. P. Leveille, Phys. Rev. **D22** (1980) 715; N. Sakai, Phys. Rev. **D22** (1980) 2220; T. Inami and T. Kubota, Nucl. Phys. **B179** (1981) 171. M. Drees and K. Hikasa, Phys. Lett. **B240** (1990) 455.

[20] OPAL Collab., M. Z. Akrawy *et al.*, Zeit. Phys **C47** (1990) 505.

[21] J. Chrin, Annals New York Acad. Sci. 535 (1988) 131.

Tables

Table 1: Centre-of-mass energies and integrated luminosities for the data in this analysis. Integrated luminosity is denoted by (OLD) for data to which the previously published analyses are applied and (NEW) for that used for the present analysis.

E_{cm} (GeV)	$OLD_{\nu\bar{\nu}H^0}$ $\int \mathcal{L}dt\ (nb^{-1})$	$NEW_{\nu\bar{\nu}H^0}$ $\int \mathcal{L}dt\ (nb^{-1})$	$OLD_{l^+l^-H^0}$ $\int \mathcal{L}dt\ (nb^{-1})$	$NEW_{l^+l^-H^0}$ $\int \mathcal{L}dt\ (nb^{-1})$	$NEW_{\tau^+\tau^-q\bar{q}}$ $\int \mathcal{L}dt\ (nb^{-1})$
88.2	33	573	124	478	606
89.2	40	670	67	626	710
90.2	44	473	108	410	517
91.2	241	3909	595	3535	4150
92.2	57	525	89	484	582
93.2	13	690	106	597	704
94.2	101	634	180	554	735
95.0	0	18	18	0	18

Table 2: Effects of the cuts for the $\nu\bar{\nu}H^0$ search channel. The cuts are described in the text.

Cut	Events in Data	Efficiency for $m_{H^0} = 40$ GeV/c^2
A0) *Preselection*	121010	77%
A1) $\theta_{acop} > 16°$	852	70%
A2) $\theta_{acol} > 26°$	98	63%
A3) $p_T > 6\ GeV/c$	71	62%
A4) $E_{30} < 2\ GeV$	21	60%
A5) $(M_{hemi1} + M_{hemi2})/2 < 12.5$ GeV/c^2 or $E_{hemi2} < 3$ GeV	0	59%

Table 3: Effect of the cuts on the efficiency of the dilepton search. The cuts are described in the text.

Cut	Events in Data	40 GeV/c^2 H^0 MC ($Z^{0*} \to \mu^+\mu^-$)	40 GeV/c^2 H^0 MC ($Z^{0*} \to e^+e^-$)
lepton pairs	245	68%	68%
cut B1	0	56%	56%
cut B2	0	54%	53%

Table 4: Number of predicted events in the various search channels, for different Higgs boson masses. The efficiencies shown, $\epsilon(Z^{0*})$, combine the total experimental acceptance and detection efficiency, over the 1989 and 1990 datasets, for the various channels differentiated by the Z^{0*} decay modes.

m_H (GeV/c^2)	$\epsilon(\nu\bar{\nu})$	$N(\nu\bar{\nu})$	$\epsilon(e^+e^-/\mu^+\mu^-)$	$N(e^+e^-/\mu^+\mu^-)$	$\epsilon(\tau^+\tau^-)$	$\epsilon(q\bar{q})$	$N(\tau^+\tau^-q\bar{q})$	N_{total}
24	0.71	19.0	0.59	5.4	0.09	0.04	0.6	25.0
28	0.69	13.0	0.57	3.6	0.08	0.04	0.4	17.0
32	0.65	8.5	0.55	2.4	0.07	0.05	0.3	11.2
36	0.63	5.6	0.54	1.6	0.06	0.06	0.2	7.4
40	0.58	3.5	0.52	1.1	0.05	0.08	0.1	4.7
45	0.52	1.9	0.51	0.6	0.05	0.11	0.1	2.6
50	0.45	0.9	0.49	0.3	0.03	0.09	0.0	1.2

Figures

Figure 1: Distribution of the normalized mass in the $\nu\bar{\nu}H^0$ search for the data (points) and the Monte Carlo (histogram), (a) after applying the preselection cuts, (b) after the cuts on acoplanarity and acollinearity and (c) after the cuts on the event p_T and energy in the backward cone. The number of events in the Monte Carlo has been normalized to the luminosity. (d) The same distribution after all the cuts for a hypothetical Higgs boson with $m_{H^0} = 40$ GeV/c^2.

Figure 2: Distributions of acoplanarity angle (in degrees) for (a) data (log scale) and (b) Monte Carlo (linear scale) of a 40 GeV/c^2 Higgs boson, after the preselection cuts (A0); and of acollinearity angle (in degrees) for (c) data (log scale) and (d) Higgs boson Monte Carlo (linear scale), after applying cut A1. The histograms in (a) and (c) are the predictions of the Jetset Monte Carlo, absolutely normalized.

Figure 3: Distribution of the average hemisphere mass for: (a) data and (b) Monte Carlo for a hypothetical Higgs boson of $m_{H^0} = 40$ GeV/c^2, after applying the requirements A1) to A4) as described in the text.

Figure 4: The sum of EM versus charged energy in both 30° degree cones around the track, for: a) data; b) Monte Carlo of a 40 GeV/c^2 Higgs boson. Plots (c) and (d) are the equivalent of (a) and (b), respectively, but for a sum in two cones of 15° and 15° about the track. No cut on the hadron calorimeter energy has been applied. In (c) and (d) the track in the 45° cone was required to have an energy greater than 20 GeV while the EM and charged energy in a cone of 15° opposite the track, was required to be less than 1 GeV.

Figure 5: Expected number of events, reduced by one standard deviation in the systematic uncertainty, as a function of the Higgs boson mass. The dashed line shows the number of events expected from the channel $H^0 \to (q\bar{q}, \tau^+\tau^-)$, $Z^{0*} \to \nu\bar{\nu}$, the dotted line is the number expected from $H^0 \to (q\bar{q}, \tau^+\tau^-)$, $Z^{0*} \to (e^+e^-$ or $\mu^+\mu^-)$, and the dot-dashed line is the number expected from the $\tau^+\tau^-$ *jet- jet* analysis; the solid line is the sum of these modes. The horizontal line indicates the 95% confidence level upper limit.

OPAL

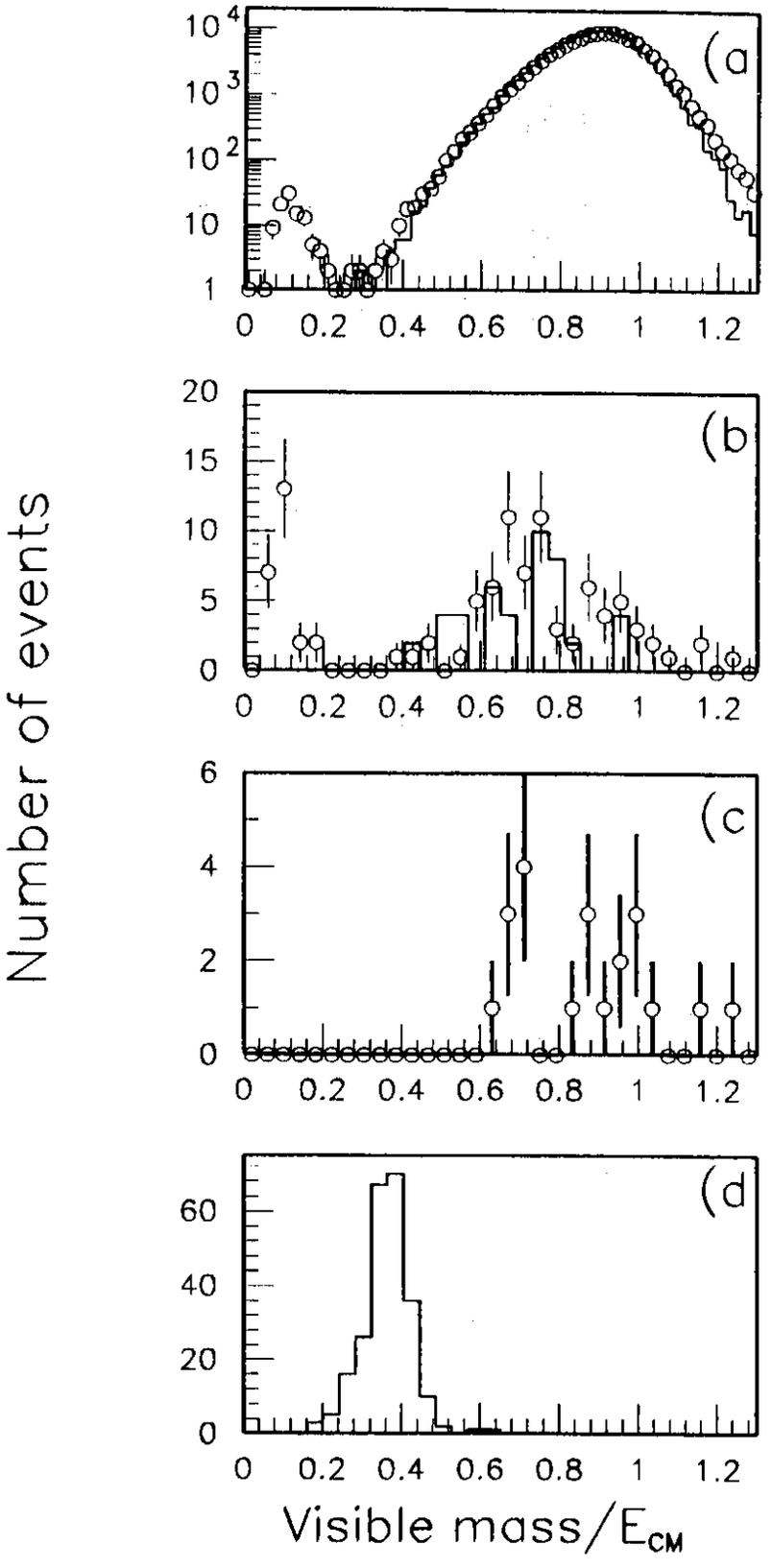

Figure 1

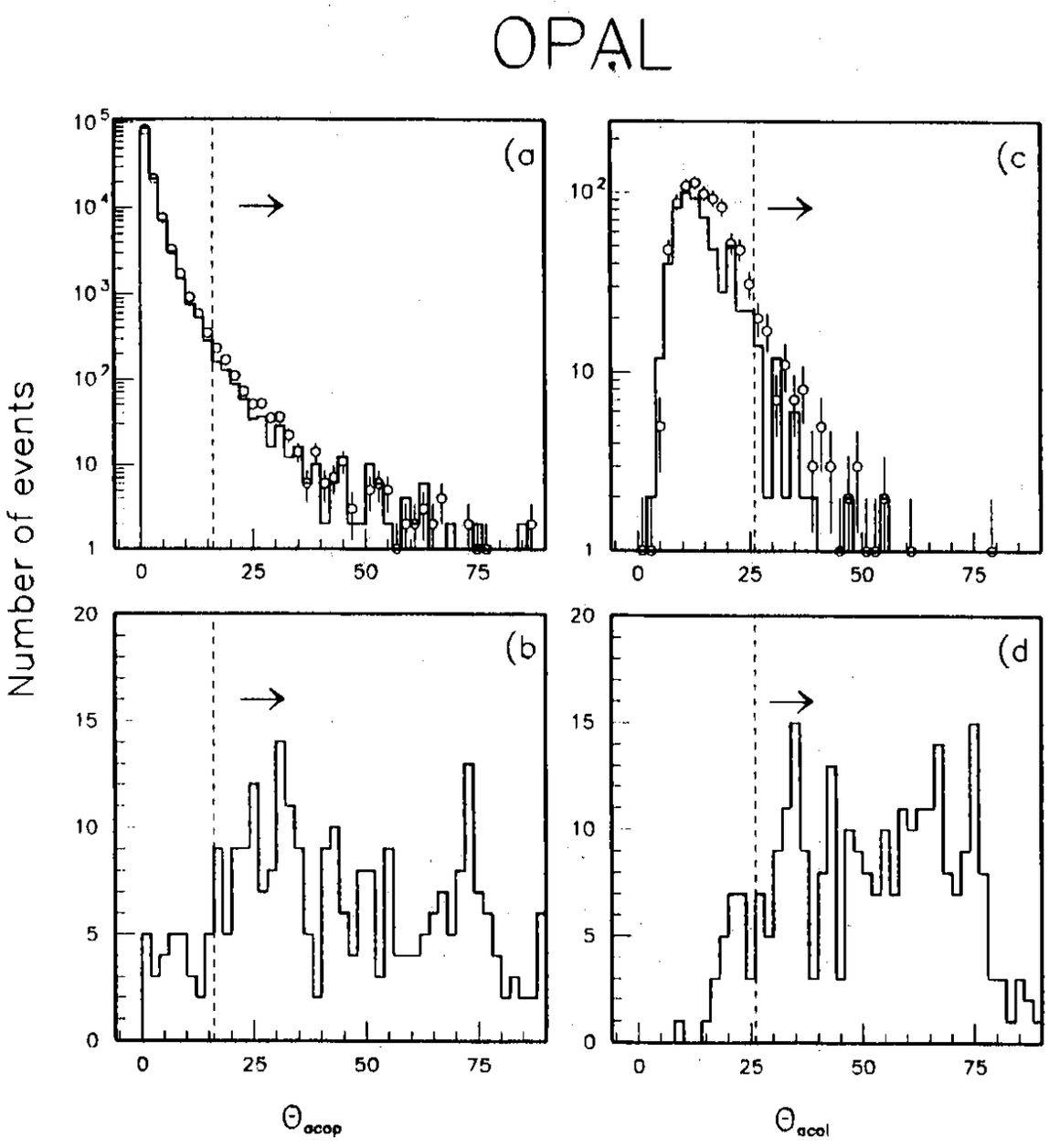

Figure 2

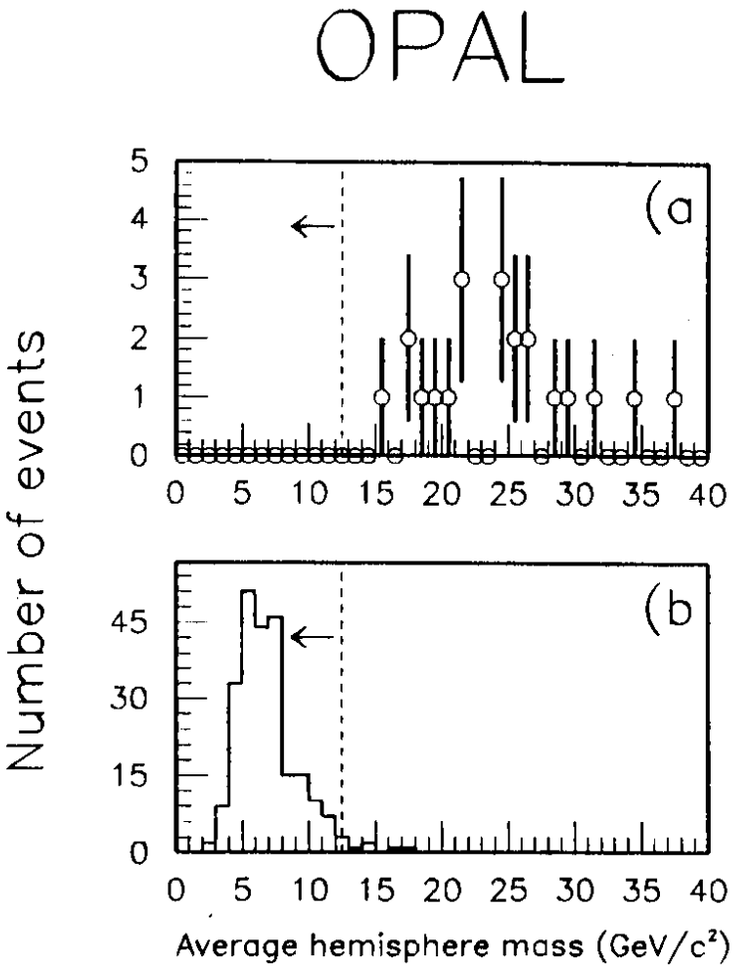
OPAL
(a)
(b)
Number of events
Average hemisphere mass (GeV/c²)
0
1
2
3
4
5
15
30
45
0 5 10 15 20 25 30 35 40

Figure 3

OPAL

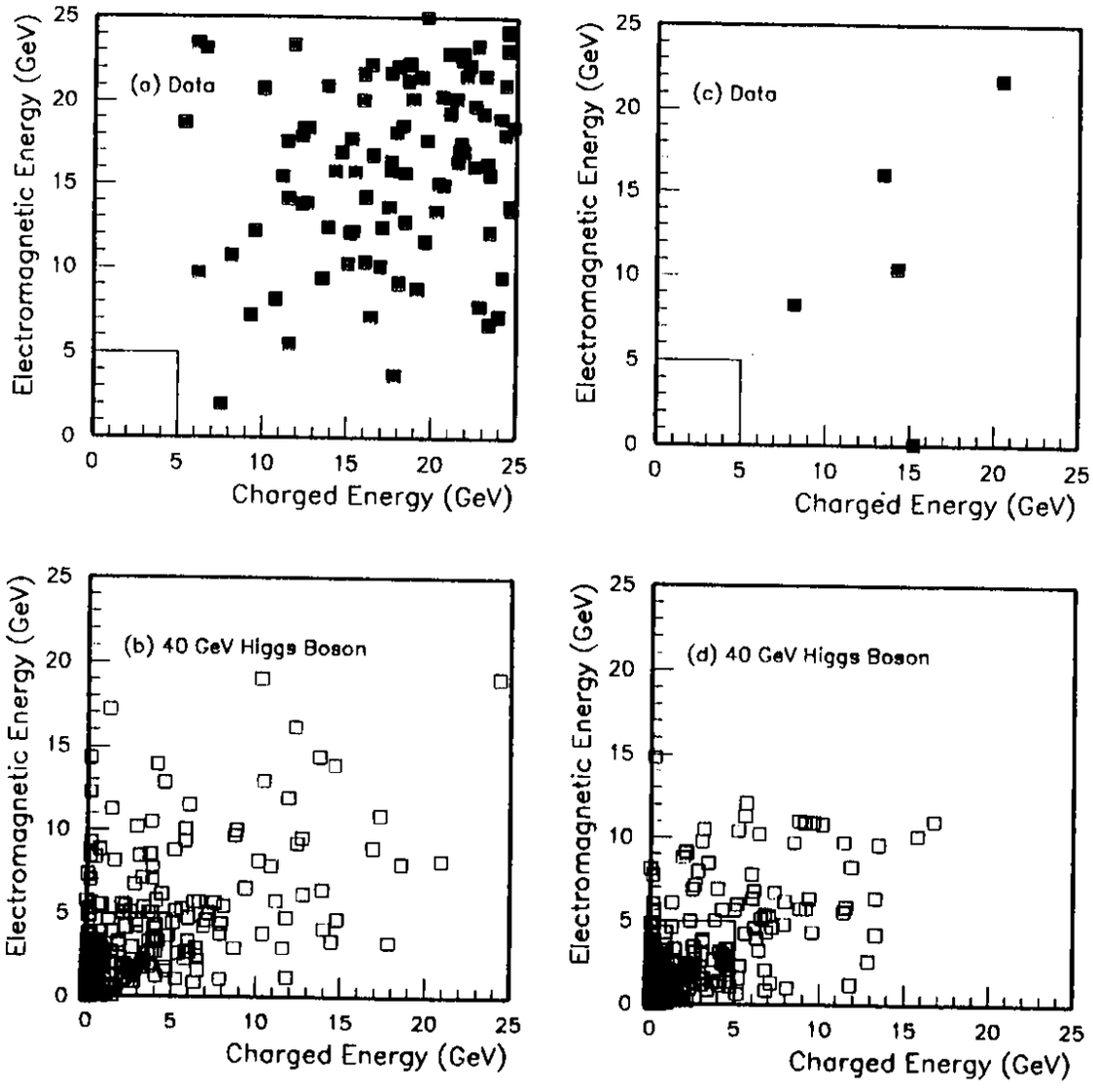

Figure 4

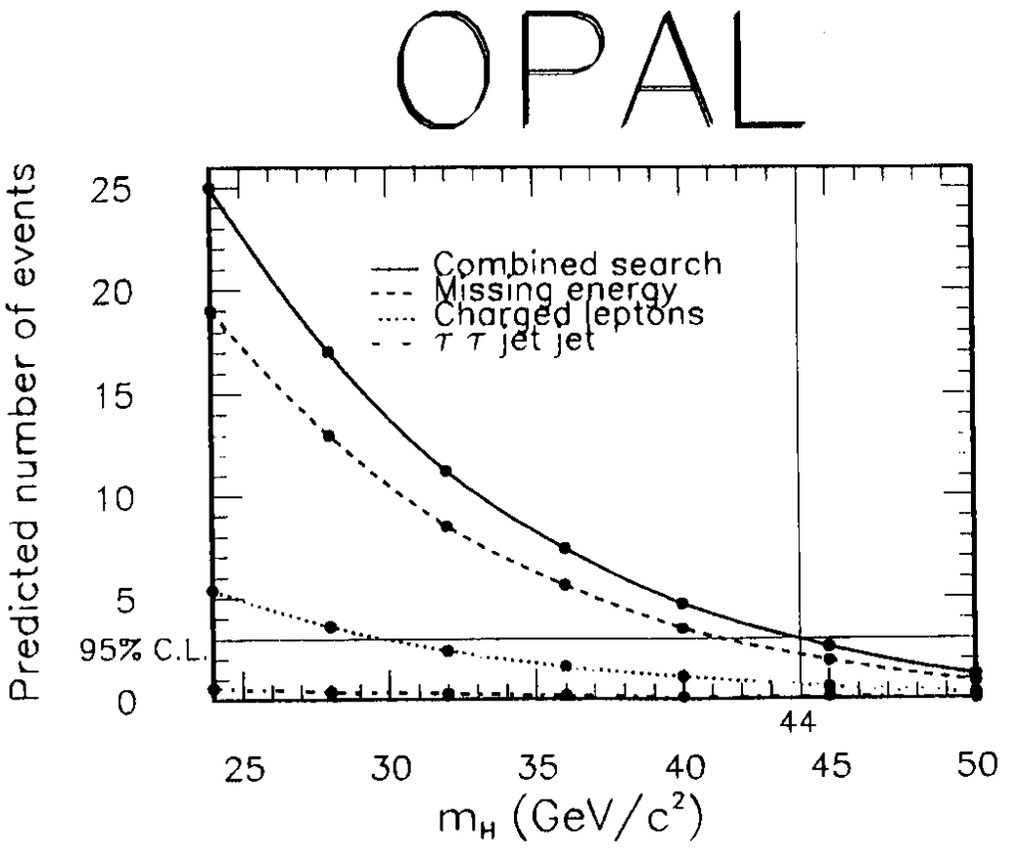

Figure 5

Imprimé au CERN. Prix : 0.70 Fr.